The Role of the Thermal Conductivity of Steel in Quantitative Elastohydrodynamic Friction

Wassim Habchi*
Department of Industrial and Mechanical Engineering, Lebanese American University
Byblos, Lebanon
wassim.habchi@lau.edu.lb

Scott Bair
Regents' Researcher
Georgia Institute of Technology, Center for High-Pressure Rheology
George W. Woodruff School of Mechanical Engineering
Atlanta, GA 30332-0405, USA
scott.bair@me.gatech.edu

*Corresponding Author

Abstract

Numerical models for thermal elastohydrodynamic lubricated contacts of steel surfaces have always employed a value for the thermal conductivity of steel corresponding to its soft annealed alloy state. However, steel in elastohydrodynamic lubricated contacts is usually hardened. It has been known for more than a century now (not within the Tribology community though) that the thermal conductivity of steel could be reduced by a factor of more than two when it is hardened. Only recently did the Tribology community realize this "mistake", of which the impact on friction predictions is investigated in this work. The mistake is found to lead to significant overestimations of friction in the thermo-viscous regime.

Keywords: elastohydrodynamic, thermal conductivity, steel surfaces, hardness

1. Introduction

Since the publication, twelve years ago, of the first elastohydrodynamic lubrication (EHL) analysis to employ real pressure and shear dependence of viscosity [1], there have been major advances in understanding the mechanisms of film formation ([2] for example) and friction generation ([3] for example) based upon primary measurements of the thermophysical properties of liquids. Until that time, full numerical simulations used properties which were adjusted to provide agreement with experiment based upon the rheological assumptions of classical EHL [4]. These assumptions require that the effect of pressure on low-shear viscosity, μ, be drastically reduced compared with viscometer measurements [4]. It has been shown that, when the pressure dependence is understated in this way, the temperature dependence must also be understated [5] to avoid the nonphysical result of viscosity decreasing with increased pressure. Thus, without an accurate description of temperature-dependent viscosity at EHL pressure, classical EHL has been unable to quantitatively evaluate the effects of the thermal properties of either the liquid or solid on the film response.

Recently the effects of micron-thick insulating coatings on EHL friction were quantitatively predicted [6] [7] from full EHL simulations employing primary measurements of the rheology and the thermal properties of the liquid at high pressure. In that work, the importance of an accurate description of shear dependent viscosity in the thermo-viscous friction regime [3] was demonstrated. The thermal conductivity of steel rollers has been assumed to be the same as that of the unhardened steel in previous analyses and in the classical approach any discrepancy with experiment could be absorbed by the adjustment of liquid properties, removing any motivation for using accurate thermal conductivity values. With the newer quantitative EHL approach, the effect of the thermal conductivity of steel may be evaluated with well-characterized reference liquids.

In 1888, Kohlrausch [8] found in comparing annealed and quenched steel bars that “The conductivity of soft steel is thus almost 80% greater than that of hard”. Today, the relationships between microstructure and thermal properties of steel are well-known [9]. Indeed, for the last thirty-five years [10] there has been much effort in non-destructive depth profiling of hardness of steel by depth profiling of thermal conductivity using the photothermal radiometric technique. A modulated laser is focused on the surface of the solid [11] to heat the surface periodically. A second probe laser detects the phase and amplitude of surface deflections. Analysis [12] then provides reconstruction of the thermal conductivity depth profile. The hardness depth profile employs a correlation between thermal and mechanical properties. It has been assumed that the thermal conductivity of hardened steel depends linearly on the hardness [10], an assumption to be employed later in this paper.

The influence of the thermal conductivity of the contacting surfaces on the performance of EHL contacts has received little attention in the Tribology literature. To the best of the authors’ knowledge, Kaneta and Yang [13] are the only ones to have investigated this issue and their

initial focus was on the influence on pressure and film thickness. They found that lower surface thermal conductivities lead to decreased film thicknesses, because of their insulating properties which induced increased film temperatures. Little influence was reported on pressure. In a later work [14], they also studied the influence on friction. They found that lower surface thermal conductivities lead to decreased friction, also because of their insulating properties. Both works though, assume that temperature dependence of the oil follows a modification of the Roelands correlation [15] [16] [17]. Thus, the temperature-viscosity coefficient, $\partial \ln \mu / \partial T$, at 30°C and only 0.6 GPa was two-thirds of the real value. As direct applications to their findings on the influence of the thermal conductivity of the solid surfaces on EHL performance, the same group of authors and their collaborators later investigated the influence on a perturbed EHL film caused by a surface feature [18], and the lubrication performance of ceramic materials [19]. The recent EHL literature has given more attention to the influence of the thermal conductivity of surface coatings – or more generally, their thermophysical properties – on lubrication performance. An experimental work by Björling et al. [20] attracted attention to the topic by reporting significantly reduced friction in Diamond-Like-Carbon (DLC) coated EHL contacts, compared to their equivalent uncoated ones, under conditions where boundary slip is unlikely to occur. The friction reduction was assumed to be the result of the insulating properties of DLC material. This assumption was later verified by a successful match of the results with numerical data [6] [7], resulting from a thermal elastohydrodynamic lubrication (TEHL) model that does not include any boundary slip effects. A localized investigation of the thermal behavior of such coated contacts further supported the assumption [21]. All the above-mentioned works on coated EHL contacts revealed the significant impact of the thermal properties of the solid surfaces – particularly their thermal conductivity – on friction, whereas little influence was reported on pressure and film thickness.

In this work, attention is directed towards the particular case of EHL contacts with steel solid surfaces. As mentioned earlier, most – if not all – numerical and analytical models of such contacts in the EHL literature (including the authors' own previous works [3][6][21][22][23]) employed a value for the thermal conductivity of steel that corresponds to its unhardened state e.g. [20][24][25][26][27][28][29][30]. This "mistake" has existed over the years despite two well-known facts. First, it has been known for more than a century [8] now (not within the Tribology community though) that this value could be reduced by a factor of more than two when steel is hardened. Second, steel rollers employed in EHL contacts (be it in an experimental setup or real-life machine component) are usually hardened. The Tribology community realized the mistake only recently, through an investigation by Reddyhoff et al. [31] of the thermal conductivity of typical tribological materials. The investigation confirmed the reduced value of the thermal conductivity of hardened steel, as compared to the often-employed value of the soft annealed alloy. The current work aims at revealing, with the new quantitative EHL approach, the significant impact of this mistake on EHL friction predictions, especially in the thermo-viscous regime [3].

2. Steel Thermal Conductivity

The thermal conductivity of the hardened steel used in bearings, cams and gears undergoing elastohydrodynamic lubrication has been assumed in classical simulations to be $k \approx 46\,\mathrm{W/m \cdot K}$, typical of steel in the annealed condition. However, for the steel in the hardened condition, which is required for elastic response to EHL level contact stress, the thermal conductivity is much less, typically $k \approx 21\mathrm{W/m \cdot K}$ [9]. Heat capacity is less dependent on heat treatment than is conductivity [9] and will thus be assumed constant throughout this work. This can be shown by the data of [9] for heat capacity of unalloyed and alloyed steels after various thermal treatments. In figure 1 below, the heat capacities are plotted against hardness and clearly show that there is no effect of hardness.

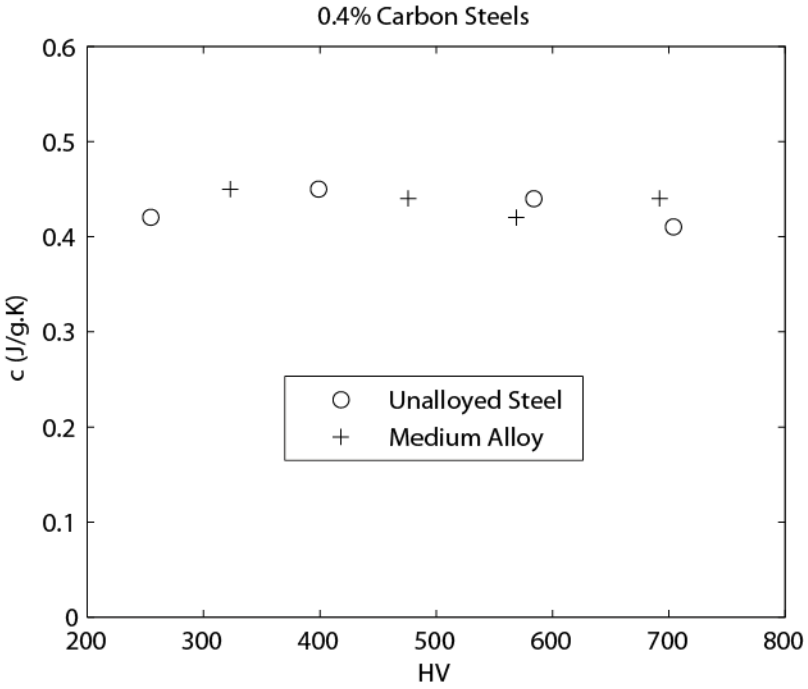

Figure 1: The heat capacity reported in [9], plotted versus hardness for two alloys

	3 hours	1.5 hours	<<1.5 hours (Hypothetical)
H_1 (HV)	800	800	800
H_2 (HV)	350	200	170
d_c (mm)	0.5	0.2	0.1
m	-1.2	-0.8	-2.0
k_s (W/m·K)	54	54	54
k' (W/m·K·HV)	0.0417	0.0417	0.0417

Table 1: Parameters of the power law expression of equation (1) for AISI 5115 steel hardness as a function of depth and the thermal conductivity linear expression of equation (2) as a function of hardness for all considered hardened steel cases

Bearing steels are either through-hardening or case-hardening. Through-hardening steels, like AISI 52100 have sufficient carbon to reach the full hardness capability, while case-hardening

steels do not. Case-hardening of steel depends on its carburizing conditions (temperature, time, etc.) [32]. Carbon is absorbed at the surface exposed to the carburizing medium and diffuses deeper with time towards the interior. The steel is then quenched to produce the hard structure. Through-hardening alloys already contain sufficient carbon to reach high hardness throughout.

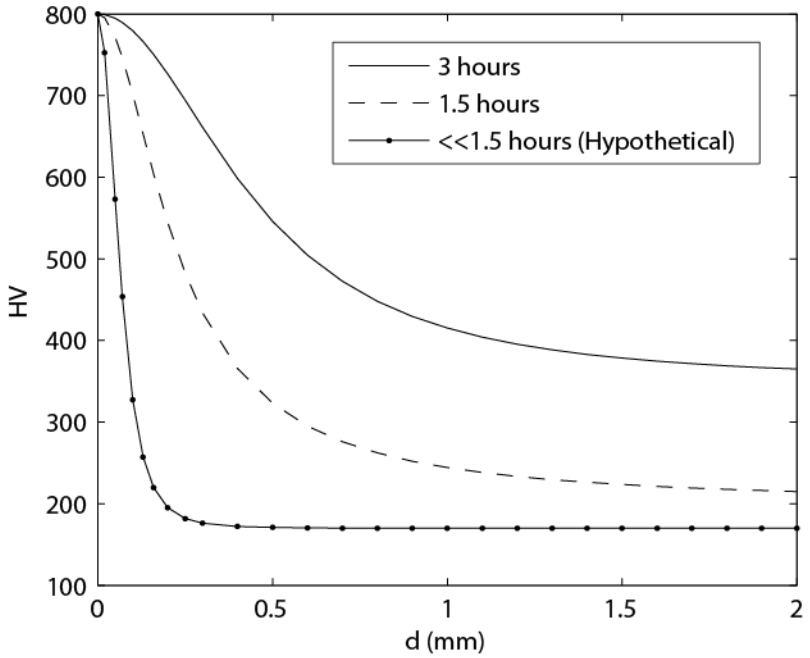

Figure 2: AISI 5115 steel Vickers Hardness variation with depth for different carburizing conditions

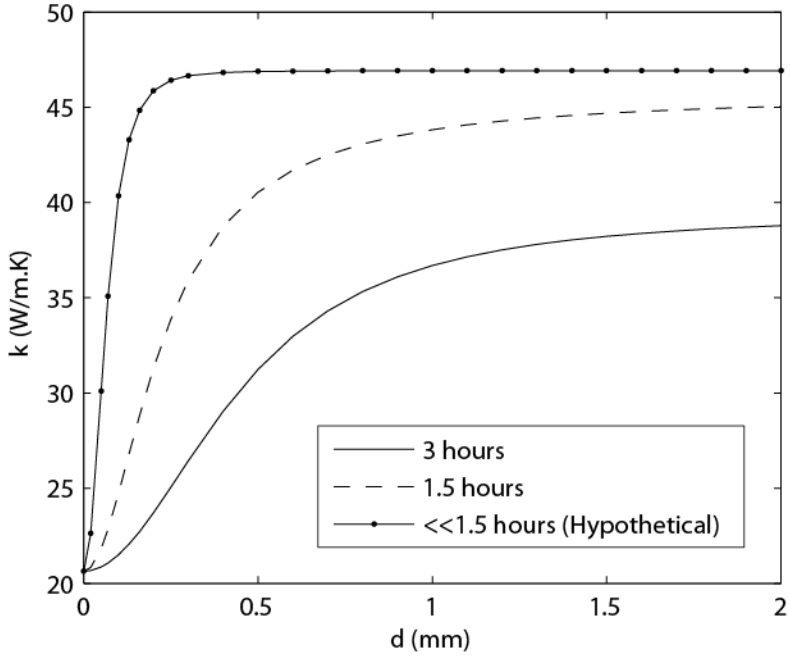

Figure 3: AISI 5115 steel thermal conductivity variation with depth for different carburizing conditions

For the current work, hardness data for carburized AISI 5115 was retrieved from [32], for two carburizing times (1.5 and 3 hours) under a temperature of 930ºC. The data was curve-fitted

to the following power-law expression of hardness H, in units of Vickers Pyramid Number (HV), as a function of depth d:

$$H = H_2 + \left(H_1 - H_2\right)\left[1 + \left(\frac{d}{d_c}\right)^2\right]^m \tag{1}$$

The fitted curves are shown in figure 2, where an additional hypothetical case was considered with a very short carburizing time, such that the carbon-rich region would be restricted to the surface of the solid, namely the top 250 microns. The parameters of equation (1) for all three considered cases are listed in table 1. Note that the hardness of the annealed steel is about 200 HV and that of the quenched steel reaches up to 800 HV with the addition of carbon. The carbon enters the steel from the carburizing medium through the surface so that there is sufficient carbon in the surface to reach 800 HV, and as carburizing time is increased, the carbon diffuses deeper towards the interior of the solid. The assumption of a linear dependence of the thermal conductivity k of hardened steel on hardness H [10] is adopted here, going from the value of the annealed state to that of the fully-hardened state. The assumption is based on the fact that Boubaker et al. [11] provide experimental evidence of a linear dependence of thermal diffusivity (i.e. the ratio of thermal conductivity to volumetric heat capacity) of steel on hardness. But, experiments by Wilzer et al. [9] reveal little dependence of the volumetric heat capacity of steel on hardness. Also, figure 3 of Walther et al. [33] clearly shows a linear relation between conductivity and hardness. Therefore, it is safe to assume that the thermal conductivity of steel varies linearly with hardness. The linear expression is given by:

$$k = k_s - k'H \tag{2}$$

The parameters of equation (2) for all three considered hardened steel cases are also listed in table 1 and the corresponding thermal conductivity variations with depth are shown in figure 3. Note that, like the hardness increase, thermal conductivity decreases first to the hardened value at the surface, and as carburizing time is increased, the decrease spreads deeper and deeper towards the interior. Also, for the hypothetical case, the decrease in thermal conductivity is restricted to the top 250-micron layer of the solid surface.

3. Numerical Methodology

The numerical model employed here is based on the full-system finite element approach [34]. A circular contact configuration is considered, for which the geometry can be reduced to that of an equivalent contact between a ball and a flat plane, as shown in figure 4.

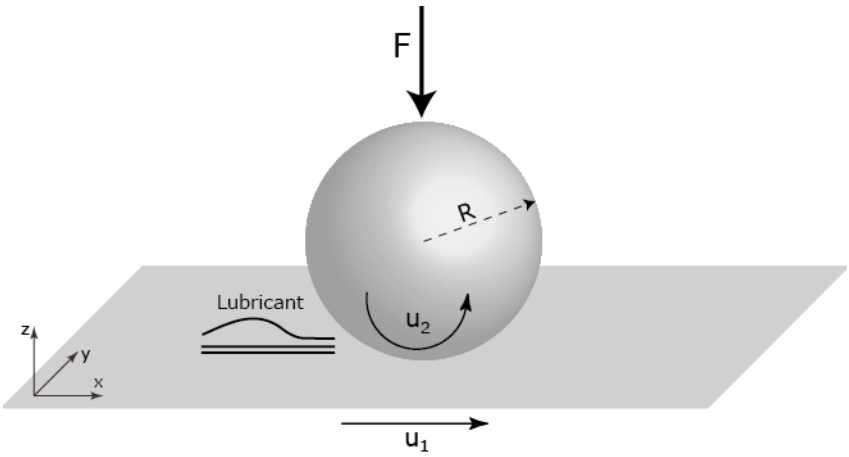

Figure 4: Equivalent geometry of a circular contact

A smooth steady-state TEHL circular contact framework is employed, as described in details in [22], with the only difference that the thermal conductivity of the contacting solids is allowed to vary with depth, according to the relations provided in equations (1) and (2). In summary, starting from a well-defined initial guess for pressure, film thickness and temperature distributions, the EHL part consisting of the generalized Reynolds, linear elasticity and load balance equations is solved in a fully-coupled way to find updated pressure and film thickness profiles, for a fixed temperature distribution. Then, the thermal part is solved, consisting in the energy equation, applied to the lubricant film and bounding solids, to find an updated temperature distribution within the solids and lubricant film, using the latest obtained pressure and film thickness profiles from the solution of the EHL part. This procedure is repeated until pressure, film thickness and temperature solutions are converged. Note that the use of the generalized Reynolds equations enables the incorporation of lubricant generalized-Newtonian behavior into the analysis i.e. the shear-dependence of lubricant viscosity. For further details about the numerical modelling subtleties (e.g. meshing, element types, convergence criteria, detailed algorithms, etc.), the reader is referred to [22] [34].

4. Results

Smooth steady-state steel-steel circular contacts are considered throughout this work, with unidirectional surface velocities, in the entrainment direction, x. A well-characterized lubricant is selected for the study, namely Shell T9, for which different thermophysical properties were measured and fitted to appropriate mathematical models in [23]. In fact, its viscosity-shear dependence as well as its low-shear viscosity, density, thermal conductivity and heat capacity dependencies on pressure and temperature were characterized. The last two were shown to be crucial for an accurate prediction of friction at high slide-to-roll ratio (i.e. the ratio of sliding speed, u_s, to the mean entrainment speed, u_m) [23]. The fluid parameters and characteristics will not be detailed here, and the interested reader is referred to [23] for more details. As for the solid properties and operating conditions, they are provided in table 2. The mechanical properties of the steel solids are assumed constant, taken at the values of the through-hardened state (AISI

52100), though it should be acknowledged that these may exhibit some dependence on hardness, temperature, etc. Such dependencies and their influence on lubrication performance are beyond the scope of the current work.

Steel Properties		Operating Conditions	
Young's Modulus:	E = 210 GPa	Ball Radius:	R = 10.32 mm
Poisson Coefficient:	υ = 0.3	Applied Load:	F = 50 N
Density:	ρ = 7810 kg/m^3	Hertz Pressure:	p_h = 1.07 GPa
Heat Capacity:	c = 475 J/kg·K	Mean Entrainment Speed:	u_m = 0.5 and 3.0 m/s
		Ambient Temperature:	T_o = 40°C
		Slide-to-Roll Ratio:	$0 \leq SRR \leq 1$

Table 2: Solid material properties and operating conditions

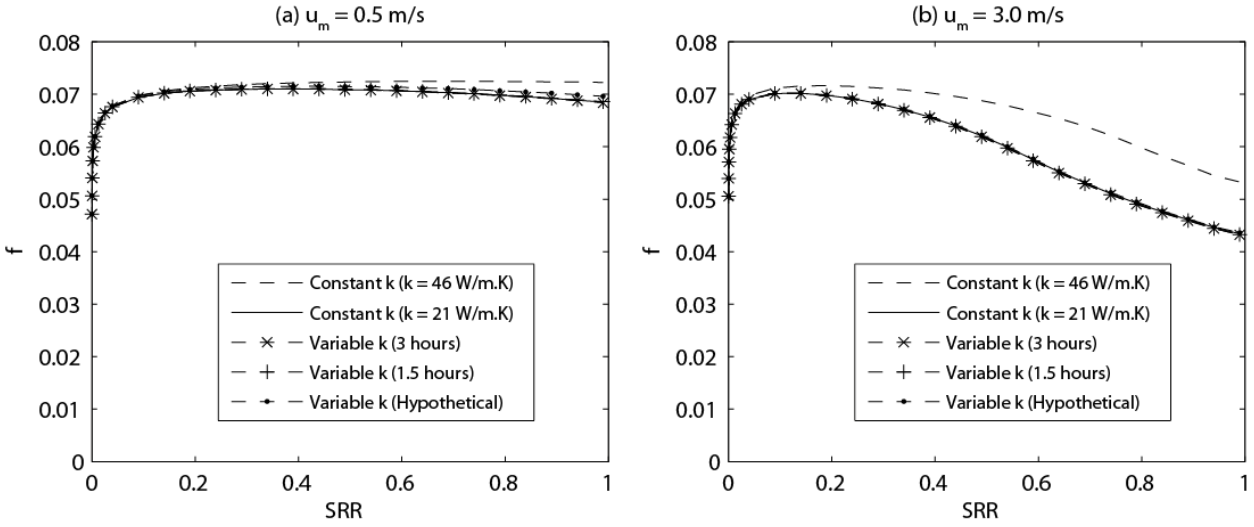

Figure 5: Friction curves for all considered steel thermal conductivity configurations, for two mean entrainment speeds: (a) u_m = 0.5 m/s and (b) u_m = 3.0 m/s

Note that the thermal conductivity of steel was not specified in Table 2. This is because five different corresponding configurations are considered: two with a constant thermal conductivity, taken either at the value of the annealed state ($k = 46\,\mathrm{W/m \cdot K}$) or that of the fully hardened state ($k = 21\,\mathrm{W/m \cdot K}$) and three with a thermal conductivity that varies with depth, for three different carburizing times (3 hours, 1.5 hours and a hypothetical case with a very short carburizing time), as detailed in section 2. The friction curves for the five different thermal conductivity configurations are reported in figure 5, for the two considered mean entrainment speed conditions. These curves show the variations of the global friction coefficient f with the slide-to-roll ratio SRR, which definitions are given by:

$$f = \frac{\int_{\Omega_c} \tau_{zx}\big|_{mid-layer}\, d\Omega}{F} \qquad \text{and} \qquad SRR = \frac{u_s}{u_m} = \frac{u_2 - u_1}{\frac{u_1 + u_2}{2}} \tag{3}$$

where u_1 and u_2 correspond to the surface velocities of the flat plane and ball, respectively, and τ_{zx} is the fluid shear stress in the *x*-direction within a plane having z as the normal direction (i.e. the *xy*-plane, which also corresponds to the contact plane). The friction coefficient is defined as the ratio of the friction force to the contact applied load, F, with the former being obtained by integrating τ_{zx} over the contact domain Ω_c, within the mid-layer of the lubricant film.

Figure 5 reveals a significant reduction in friction at high SRR for hardened steel compared to the soft annealed alloy, irrespective of the carburizing time, and that the reduction is amplified with increasing mean entrainment speed. In fact, for the low speed case (figure 5a), the relative decrease at $SRR = 1$ between the two extreme cases; that is, the soft case ($k = 46\,\mathrm{W/m \cdot K}$) and the fully-hardened case ($k = 21\,\mathrm{W/m \cdot K}$) is 5.2%, whereas for the high speed case (figure 5b), it is 18.5%. Figure 5 also reveals that carburizing time has little to no influence on the friction reduction; except for the low speed case (figure 5a) where a minor effect is observed for the hypothetical case, exhibiting a relative increase in friction with respect to the fully-hardened case of 1.6%, at $SRR = 1$. Note that the influence of the solid thermal conductivity on friction is rather limited for the low-to-medium sliding regime ($SRR < 0.2$); a regime encountered in the operation of roller bearings or spur gears, for example. Next, the underlying physics behind these observations are investigated and discussed.

5. Discussion

It was shown in section 4 that the common "mistake" of using the thermal conductivity of steel in the annealed state for the analysis of steel-steel TEHL contacts – which usually employ hardened steel instead – can lead to a significant overprediction of friction in the thermo-viscous regime (at high slide-to-roll ratios). This is because the thermal conductivity of hardened steel is generally much lower than that of soft steel (as discussed in section 2); which gives it an insulating effect. This fact is revealed through figure 6 which shows the total heat fluxes $q = \int_{\Omega_c} k\,\partial T/\partial n\, d\Omega$ (where n is the normal direction to the solid surfaces) passing from the fluid film towards the solids (ball and plane), through the fluid-solid interfaces, for the two extremities of the solid thermal conductivity configurations; that is, the soft case ($k = 46\,\mathrm{W/m \cdot K}$) and the fully-hardened case ($k = 21\,\mathrm{W/m \cdot K}$). Note that convective heat flux is nil since solid surface velocities are parallel to the fluid-solid interfaces and as such, they have a zero normal component. Thus, the heat flux traversing the fluid-solid interfaces is purely conductive.

First, figure 6 reveals that, for a given thermal conductivity configuration, the heat flux traversing the ball is always greater than the one going through the plane, irrespective of the mean entrainment speed or the slide-to-roll ratio. This is because the ball is moving faster than the plane under the considered operating conditions ($SRR > 0$) and can thus transport more heat by mass from the contact region. Second, for the high mean entrainment speed case (figure 6b)

the amount of heat going through the solids is greater than for the low mean entrainment speed case (figure 6a) for a given thermal conductivity configuration and a given slide-to-roll ratio, because of the increased heat generation by shear. If more heat is generated within the lubricant film, then more heat will be dissipated through the solid surfaces. Finally, and most importantly, hardened steel exhibits an insulating effect, leading to lower heat dissipation through the fluid-solid interfaces compared to soft steel, irrespective of the operating conditions. This translates into higher lubricant film temperatures, as can be seen in figure 7.

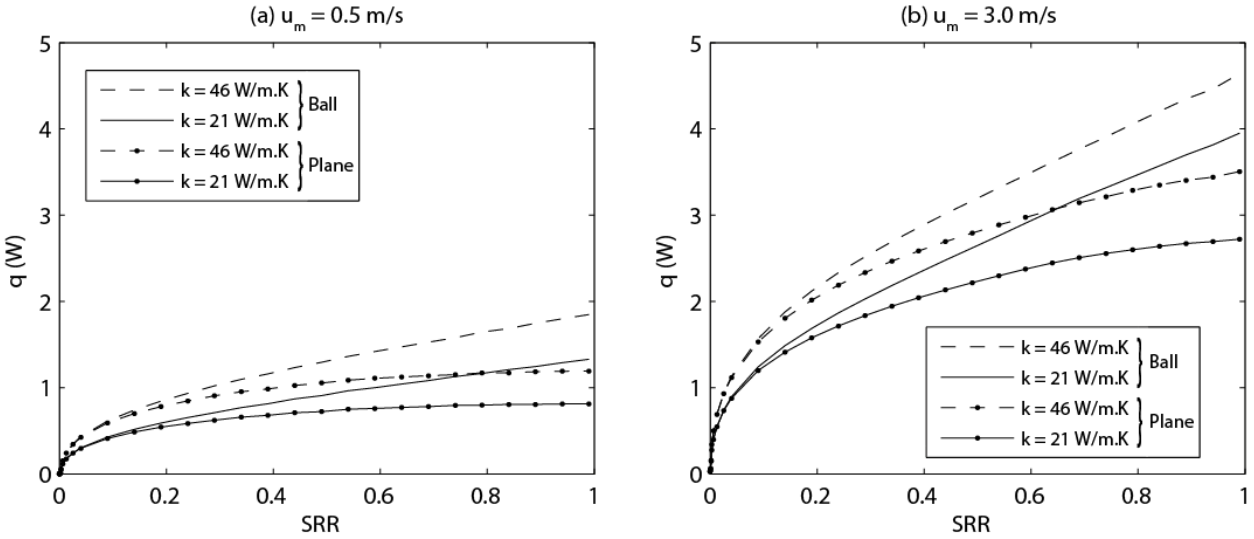

Figure 6: Total heat flux through the soft annealed (k = 46 W/m·K) and through-hardened (k = 21 W/m·K) steel surfaces, for two mean entrainment speeds: (a) u_m = 0.5 m/s and (b) u_m = 3.0 m/s

In fact, figure 7 shows the temperature rise $\Delta T = T - T_0$ across the lubricant film in the z-direction at the contact center for $SRR = 0.2$ and $SRR = 1.0$, for the two thermal conductivity configurations, for the two considered mean entrainment speeds. Note that $Z = z/h$ (where h is the lubricant film thickness) defines the dimensionless space coordinate in the z-direction. Within the lubricant film, Z varies from zero to unity; with $Z = 0$ corresponding to the plane surface, while $Z = 1$ corresponds to the ball surface. First, note that the temperature rise over the plane surface is higher than that over the ball surface irrespective of the mean entrainment speed, the slide-to-roll ratio or the thermal conductivity configuration because, as mentioned earlier, the ball is moving faster ($SRR > 0$). Thus, it can carry more heat by mass out of the contact, leading to the observed lower film temperatures at its surface. Consequently, the temperature differential between the fluid film and the ball surface is higher than between the fluid film and the plane surface, which leads to the higher heat fluxes going through the ball, revealed in figure 6. Second, for the high mean entrainment speed case (figures 7b and 7d), for a given *SRR*, the temperature rise within the film is higher than for the corresponding low mean entrainment speed cases (figures 7a and 7c), because of the increased heat generation by shear mentioned earlier. Finally, and most importantly, because of its higher insulating capabilities, hardened steel leads to increased lubricant film temperatures compared to soft steel, irrespective of the mean

entrainment speed and slide-to-roll ratio. This explains its lower friction characteristics reported in figure 5, since the increased film temperatures would lead to reduced lubricant viscosity. Note that this last statement is only true under full-film EHL conditions. In the mixed-EHL regime, when surface roughness is included, increased film temperatures would result in lubricant viscosity reductions that may lead to more asperity-asperity contact and thus, increased friction.

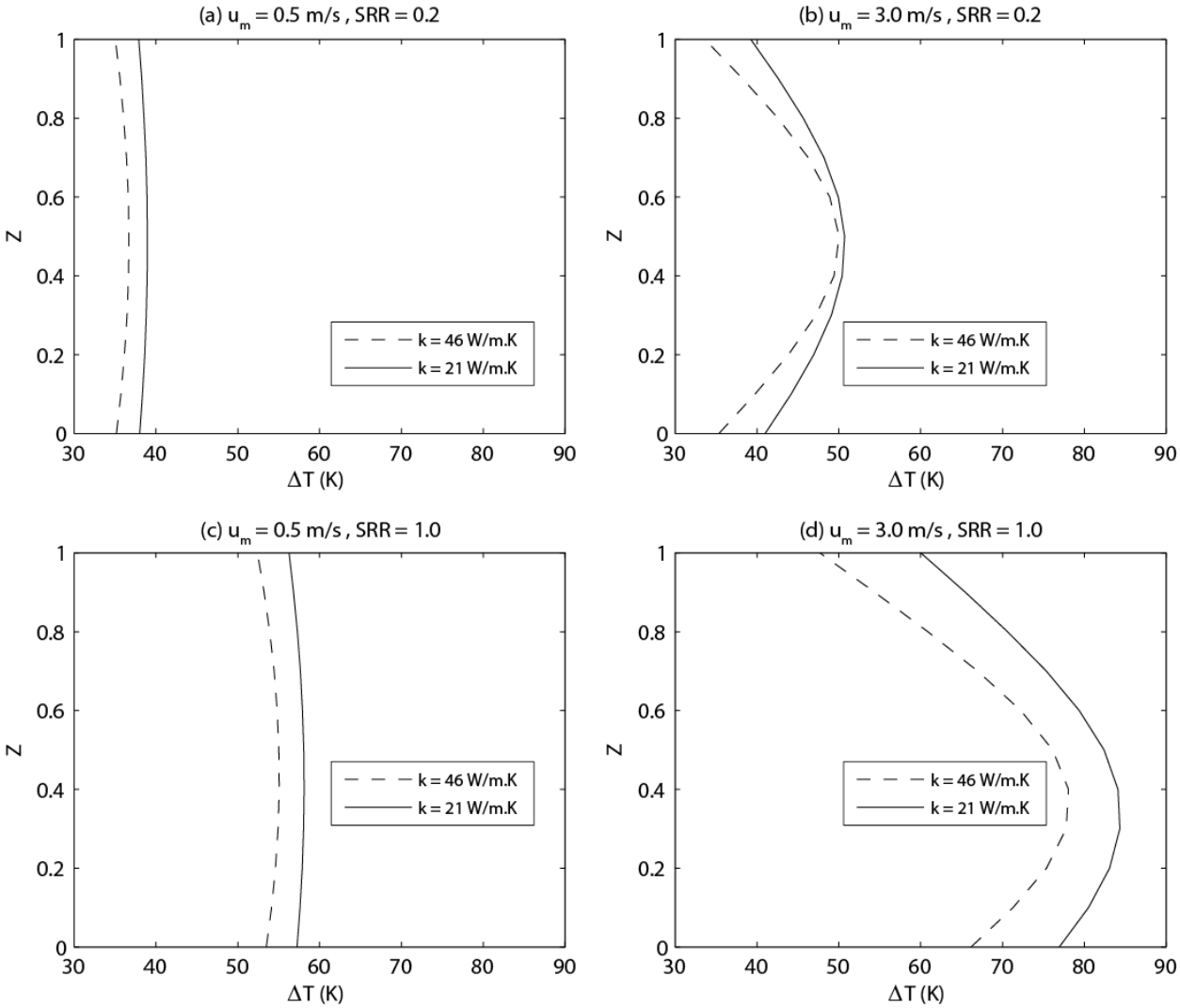

Figure 7: Temperature rise across the lubricant film at the contact center for soft annealed (k = 46 W/m·K) and through-hardened (k = 21 W/m·K) steel surfaces: (a) u_m = 0.5 m/s, SRR = 0.2; (b) u_m = 3.0 m/s, SRR = 0.2; (c) u_m = 0.5 m/s, SRR = 1.0 and (d) u_m = 3.0 m/s, SRR = 1.0

In section 4, it was also revealed that carburizing time had little to no influence on the friction reduction between the soft and hard steel cases; except for the low speed case where a minor effect was reported for the hypothetical thermal conductivity configuration. To understand this, the heat penetration depth within the two solids is investigated. For this, figure 8a and figure 8b show the temperature rise at the contact center within the interior of the ball and plane, respectively, for the low mean entrainment speed case ($u_m = 0.5\,\mathrm{m/s}$), for $SRR = 1$, for all five

considered thermal conductivity configurations. Clearly, because of the higher thermal conductivity of soft steel, heat penetrates deeper within the corresponding solids i.e. temperature rise becomes nil at higher depth. Also, given the lower surface speed of the plane, heat penetrates deeper within its interior than that of the ball, irrespective of the thermal conductivity configuration. This is attributed to its reduced heat removal by mass (advection), compared to the ball. Also note that a higher temperature rise within the interior of the solids generally implies a lower temperature rise within the corresponding lubricant film (see figure 7). This is because more of the heat generated within the film has been transferred towards the solids, increasing their temperature and reducing that of the film. Finally, note that for both the ball and the plane, for the four hardened steel thermal conductivity configurations, heat does not penetrate beyond a depth of 200 microns; except for the hypothetical case, where a small temperature rise could be observed at this depth, within the plane. This explains the slight friction deviation between the hypothetical case and the other three hardened steel configurations, reported in section 4. In fact, below a depth of 200 micron, the deviation in thermal conductivity of the cases with 3 hours and 1.5 hours of carburization time from that of the fully-hardened case is rather limited (see figure 3). Therefore, their frictional response is virtually the same, as can be seen in figure 5. Only the hypothetical case exhibits a significant thermal conductivity deviation from that of the fully-hardened case at a depth of 200 micron, with a thermal conductivity almost reaching that of the soft annealed state. Thus, its frictional response slightly differs from that of the other three hardened cases (see figure 5a). Note that this is only true for the low speed case (figure 5a), while for the high-speed case (figure 5b) the difference is negligible. This is because, as discussed earlier, heat penetration depth decreases with increased surface speed, reducing this effect.

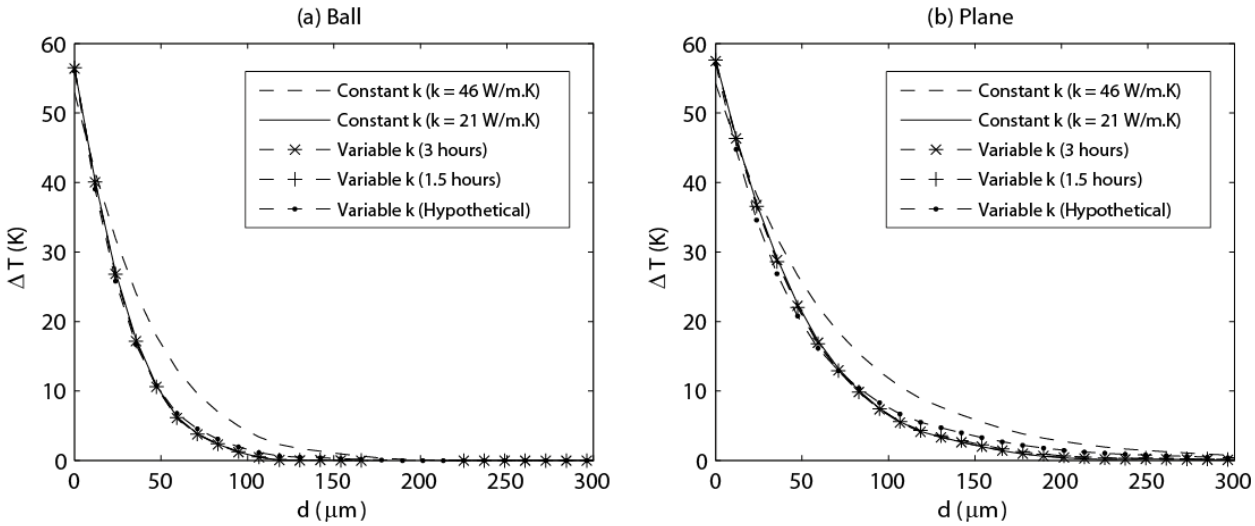

Figure 8: Temperature rise at the contact center as a function of depth within: (a) the ball and (b) the plane, for all five considered thermal conductivity configurations, for u_m = 0.5 m/s and *SRR* =1

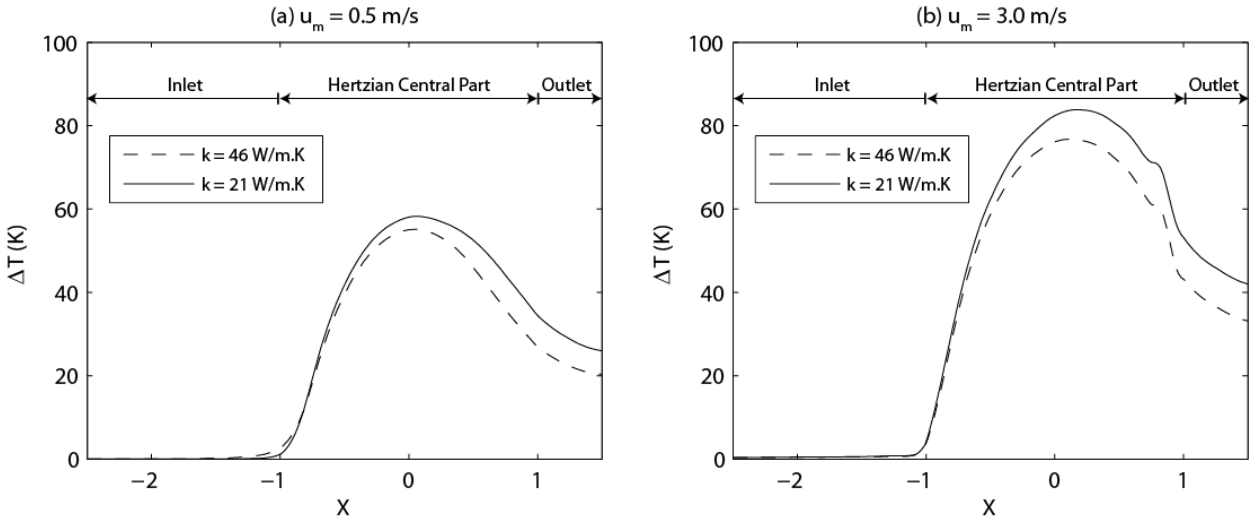

Figure 9: Temperature rise within the mid-layer of the lubricant film ($Z = 0.5$) in the entrainment direction x, for SRR =1, for soft annealed (k = 46 W/m·K) and through-hardened (k = 21 W/m·K) steel surfaces, for two mean entrainment speeds: (a) u_m = 0.5 m/s and (b) u_m = 3.0 m/s

Finally, note that throughout this work, the discussion was limited to the influence of steel thermal conductivity on frictional performance, with no mention of the influence on film build-up performance. This is because, under the considered operating conditions, relative deviations in lubricant film thickness turned out to be rather limited (below 1%), between all five considered thermal conductivity configurations. This is attributed to the fact that the corresponding differences in temperature rise within the film are confined to the central and outlet regions of the contact and they do not diffuse towards the inlet region, as can be seen in figure 9. In fact, figure 9 shows the temperature rise within the mid-layer of the lubricant film ($Z = 0.5$) along the central line of the contact in the entrainment direction x, for the two considered mean entrainment speeds, for $SRR = 1$, for the two extremities of the solid thermal conductivity configurations; that is, the soft annealed case ($k = 46\,\mathrm{W/m \cdot K}$) and the fully-hardened case ($k = 21\,\mathrm{W/m \cdot K}$). Note that $X = x/a$ (where a is the Hertzian contact radius) defines the dimensionless space coordinate in the x-direction. Clearly, differences in temperature rise between the two thermal conductivity configurations do not diffuse towards the inlet region of the contact, which is known to govern film build-up. The differences remain confined to the central / Hertzian and outlet regions of the contact. Since the former is known to govern the frictional response of the contact, this leads to substantial deviations in friction only.

6. Conclusion

Numerical models for TEHL contacts of steel surfaces have always employed a value for the thermal conductivity of steel that corresponds to its soft annealed alloy state ($k = 46\,\mathrm{W/m \cdot K}$). However, steel EHL contacts in test rigs or real machine elements are usually hardened. It has been known for more than a century now (not within the Tribology community though) that this value could be reduced by a factor of more than two when steel is hardened. Only recently did

the Tribology community realize this “mistake”, which is not without consequence on the performance prediction capability of TEHL numerical models. This work investigated the impact of this mistake on friction predictions. It was found that the use of the thermal conductivity of soft annealed steel in TEHL simulations of steel contacts leads to a significant overestimation of friction coefficients in the thermo-viscous friction regime. This was found to stem from the lower thermal conductivity of hardened steel, which offers it a higher insulating capability, leading to increased lubricant film temperatures and thus, reduced friction. Note that this last statement is only true under full-film EHL conditions. In the mixed-EHL regime, when surface roughness is included, increased film temperatures would result in lubricant viscosity reductions that may lead to more asperity-asperity contact and thus, increased friction. The increased film temperatures were found to remain confined to the central part of the contact though, which meant that the impact on film build-up was limited. Finally, carburizing time of the hardening process of steel was found to have little to no influence on friction. Therefore, for most cases, a constant thermal conductivity at the value of the fully-hardened steel ($k = 21\mathrm{W/m\cdot K}$) could be used, without compromising the accuracy of friction predictions. In fact, a detailed analysis of the heat dissipation within the depth of the solid bodies revealed that the lower thermal conductivity of hardened steel meant a shallower heat penetration within the solids. For all considered carburizing times though, the penetration depth remained below 200 micron; a depth below which the variations in thermal conductivity with carburizing time with respect to the fully-hardened case are rather limited.

References

[1] Liu Y., Wang Q. J., Bair S. and Vergne, P. - A quantitative solution for the full shear-thinning EHL point contact problem including traction, *Tribology Letters*, 2007, vol. 28(2), pp. 171-181.

[2] Habchi W., Bair S., Qureshi F. and Covitch M. - A film thickness correction formula for double-Newtonian shear-thinning in rolling EHL circular contacts, *Tribology Letters*, 2013, vol. 50 (1), pp. 59-66.

[3] Habchi W., Bair S. and Vergne P. - On friction regimes in quantitative elastohydrodynamics, *Tribology International*, 2013, vol. 58, pp. 107-117.

[4] Bair S. - The rheological assumptions of classical EHL: What went wrong?, *Tribology International*, 2019, vol. 131, pp. 45-50.

[5] Bair S. - A critical assessment of the role of viscometers in quantitative elastohydrodynamics, *Tribology Transactions*, 2012, vol. 55(3), pp. 394-399.

[6] Björling M., Habchi W., Bair S., Larsson R. and Marklund, P. - Friction reduction in elastohydrodynamic contacts by thin-layer thermal insulation, *Tribology letters*, 2014, vol. 53(2), pp. 477-486.

[7] Björling M., Habchi W., Bair S., Larsson R. and Marklund P. - Correction to: Friction Reduction in Elastohydrodynamic Contacts by Thin-Layer Thermal Insulation, *Tribology Letters*, 2018, vol. 66(4), p. 125.

[8] Kohlrausch F. - On the thermal conductivity of hard and soft steel, *The London, Edinburgh, and Dublin Philosophical Magazine and Journal of Science*, 1888, vol. 25(156), pp. 448-450.
[9] Wilzer J., Lüdtke F., Weber S. and Theisen W. - The influence of heat treatment and resulting microstructures on the thermophysical properties of martensitic steels, *Journal of Materials Science*, 2013, vol. 48(24), pp. 8483-8492.
[10] Jaarinen J. and Luukkala M. - Numerical analysis of thermal waves in stratified media for non-destructive testing purposes, *Journal de physique*, 1983, vol. 44(6), pp. 503-508.
[11] Boubaker K. M., Bouhafs M. and Yacoubi N. - A quantitative alternative to the Vickers hardness test based on a correlation between thermal diffusivity and hardness – applications to laser-hardened carburized steel, *NDT & E International*, 2003, vol. 36(8), pp. 547-552.
[12] Celorrio R., Apiñaniz E., Mendioroz A., Salazar A. and Mandelis A. - Accurate reconstruction of the thermal conductivity depth profile in case hardened steel, *Journal of Applied Physics*, 2010, vol. 107(8), 083519.
[13] Kaneta M. and Yang P. - Effects of thermal conductivity of contacting surfaces on point EHL contacts, *ASME Journal of Tribology*, 2003, vol. 125, pp. 731-738.
[14] Kaneta M. and Yang P. - Effects of the thermal conductivity of contact materials on elastohydrodynamic lubrication characteristics, *IMechE Part C: Journal of Mechanical Engineering Science*, 2010, vol. 224(12), pp. 2577-2587.
[15] Bair, S. - Measurements of real non-Newtonian response for liquid lubricants under moderate pressures, *IMechE Part J: Journal of Engineering Tribology*, 2001, vol. 215(3), pp. 223-233.
[16] Bair S. – Discussion: "Quantitative comparisons between measured and solved EHL dimples in point contacts," (Yang P., Kaneta M. and Masuda S., 2003, ASME J. of Tribology, 125(1), pp. 210-214), *ASME Journal of Tribology*, 2005, vol. 127, p. 456.
[17] Yang P., Kaneta M. and Masuda S. – Closure to "Discussion: 'Quantitative comparisons between measured and solved EHL dimples in point contacts,' (Yang P., Kaneta M. and Masuda S., 2003, ASME J. of Tribology, 125(1), pp. 210-214)", *ASME Journal of Tribology*, 2005, vol. 127, p. 457.
[18] Kaneta M., Cui J., Yang P., Krupka I. and Hartl M. - Influence of thermal conductivity of contact bodies on perturbed film caused by a ridge and groove in point EHL contacts. *Tribology International*, 2016, vol. 100, pp. 84-98.
[19] Kaneta M., Sperka P., Yang P., Krupka I., Yang P. and Hartl. M. - Thermal elastohydrodynamic lubrication of ceramic materials, *Tribology Transactions*, 2018, vol. 61(5), pp. 869-879.
[20] Björling M., Isaksson P., Marklund P. and Larsson R. – The Influence of DLC Coating on EHL Friction Coefficient, *Tribology Letters*, 2012, vol. 47, pp. 285-294.
[21] Habchi W. - Thermal Analysis of Friction in Coated Elastohydrodynamic Circular Contacts, *Tribology International*, 2016, vol. 93, pp. 530-538.

[22] Habchi W., Eyheramendy D., Bair S., Vergne P. and Morales-Espejel G. E. – Thermal Elastohydrodynamic Lubrication of Point Contacts Using a Newtonian/Generalized Newtonian Lubricant, *Tribology Letters*, 2008, vol. 30 (1), pp. 41-52.

[23] Habchi W., Vergne P., Bair S., Andersson O., Eyheramendy D. and Morales-Espejel G. E. – Influence of Pressure and Temperature Dependence of Thermal Properties of a Lubricant on the Behavior of Circular TEHD Contacts, *Tribology International*, 2010, vol. 43, pp. 1842-1850.

[24] Kaneta M., Yang P., Krupka I. and Hartl M. – Fundamentals of thermal elastohydrodynamic lubrication in Si_3N_4 and steel circular contacts, *IMechE Part J: Journal of Engineering Tribology*, 2015, vol. 229 (8), pp. 929-939.

[25] Raisin J., Fillot N., Dureisseix D., Vergne P. and Lacour V. – Characteristic Times in Transient Thermal Elastohydrodynamic Line Contacts, *Tribology International*, 2015, vol. 82, pp. 472-483.

[26] Hajishafiee A., Kadiric A., Ioannides S. and Dini D. - A coupled finite-volume CFD solver for two-dimensional elasto-hydrodynamic lubrication problems with particular application to rolling element bearings, *Tribology International*, 2017, vol. 109, pp. 258-273.

[27] Peng Y., Zhao N., Zhang M., Li W. and Zhou R. - Non-Newtonian thermal elastohydrodynamic simulation of helical gears considering modification and misalignment, *Tribology International*, 2018, vol. 124, pp. 46-60.

[28] Everitt C.-M. and Alfredsson B. - Surface initiation of rolling contact fatigue at asperities considering slip, shear limit and thermal Elastohydrodynamic lubrication, *Tribology International*, 2019, vol. 137, pp. 76-93.

[29] Liu Z., Pickens III D., He T., Zhang X., Liu Y., Nishino T. and Wang Q. J. – A thermal elastohydrodynamic lubrication model for crowned rollers and its application on apex seal-housing interfaces, *ASME Journal of Tribology*, 2019, vol. 141, 041501.

[30] Bobach. L, Bartel D., Beilicke R., Mayer J., Michaelis K., Stahl K. and Bachmann S. – Reduction in EHL friction by a DLC coating, *Tribology Letters*, 2015, vol. 60, 17.

[31] Reddyhoff T., Schmidt A. and Spikes H. - Thermal conductivity and flash temperature. *Tribology Letters*, 2019, vol. 67:22.

[32] Selcuk B., Ipek R., Karamiş M. B. and Kuzucu V. - An investigation on surface properties of treated low carbon and alloyed steels (boriding and carburizing), *Journal of Materials Processing Technology*, 2000, vol. 103(2), pp. 310-317.

[33] Walther, H.G., Fournier, D., Krapez, J.C., Luukkala, M., Schmitz, B., Sibilia, C., Stamm, H. and Thoen, J. (2002). Photothermal steel hardness measurements-results and perspectives. In Analytical Sciences/Supplements Proceedings of 11th International Conference of Photoacoustic and Photothermal Phenomena (pp. s165-s168). The Japan Society for Analytical Chemistry.

[34] Habchi W. - Finite Element Modeling of Elastohydrodynamic Lubrication Problems, 2018, Wiley, Chichester, UK, ISBN: 978-1-119-22512-6.